Helical Sense-Responsive and Substituent-Sensitive Features in Vibrational and Electronic Circular Dichroism, in Circularly Polarized Luminescence, and in Raman Spectra of Some Simple Optically Active Hexahelicenes

Sergio Abbate,[*,†,‡] Giovanna Longhi,[†,‡] France Lebon,[†,‡] Ettore Castiglioni,[†,§] Stefano Superchi,[||] Laura Pisani,[||] Francesca Fontana,[⊥] Franck Torricelli,[⊥] Tullio Caronna,[⊥] Claudio Villani,[#] Rocchina Sabia,[#] Matteo Tommasini,[○] Andrea Lucotti,[○] Daniele Mendola,[○] Andrea Mele,[○] and David A. Lightner[□]

[†]Dipartimento di Medicina Molecolare e Traslazionale, Università di Brescia, Viale Europa 11, 25123 Brescia, Italy

[‡] Consorzio Interuniversitario di Scienze Fisiche della Materia (CNISM), Via della Vasca Navale 85, 00100 Roma, Italy

[§] Jasco-Europe, via Cadorna 1, 23894 Cremella (LC), Italy

[||] Dipartimento di Scienze, Università della Basilicata, Via dell'Ateneo Lucano, 85100 Potenza, Italy

[⊥] Dipartimento di Ingegneria Industriale, Università di Bergamo, Viale Marconi 5, 24044 Dalmine (BG), Italy

[#] Dipartimento di Chimica e Tecnologia del Farmaco, Università degli Studi "La Sapienza", P.le Aldo Moro 5, 00185 Roma

[○] Dipartimento di Chimica, Materiali e Ingegneria Chimica "G. Natta", Politecnico di Milano, Piazza Leonardo da Vinci 32, 20133 Milano, Italy

[□] Department of Chemistry, University of Nevada, Reno, Nevada 89557, United States

I. INTRODUCTION

Since the early days of optical activity studies, hexahelicene,[1−3] which is an inherently dissymmetric molecule consisting of six *ortho*-fused benzene rings, has been regarded as an important system on which to test emerging theory and calculation of optical rotation (OR)[4,5] through the celebrated Rosenfeld formula.[6] During the past 50+ years, numerous studies have been conducted to assess assignment of the absolute configuration (AC), which was unequivocally established on the basis of the combined use of OR, of electronic circular dichroism (ECD), and of X-ray diffraction methods, studying (+)- and (−)-hexahelicene, (+)- and (−)-2-Br-hexahelicene, and (+)- and (−)-2-CH₃-hexahelicene[7−9] (in all cases the (−) optical isomer was found to be associated with the *M* helicity). The latter study pointed out that an erroneous prediction of AC had been made in refs 4 and 5. Progress in ab initio methods and use of more powerful computational routines allowed for identifying the origin of the inadequacy of the first theoretical attempt[10,11] due to the difficulty, at that time, in taking into account a sufficient number of excited states in configuration interaction.

Various synthesis and resolution studies have been conducted on hexahelicenes, see for examples refs 12−16. Among the various spectroscopic techniques, the most direct ones applicable on helicenes are the chiroptical techniques, and among these ones the most used has been ECD, which was employed on various helicenes,[7−9,17−19] helping to confirm the above findings.

Scheme 1. *P*-Configuration of Hexahelicenes Examined in This Study: 5-Aza-hexahelicene (**1**), Hexahelicene (**2**), 2-Methyl-hexahelicene (**3**), and 2-Bromo-hexahelicene (**4**)[a]

(1)   (2)   (3)   (4)
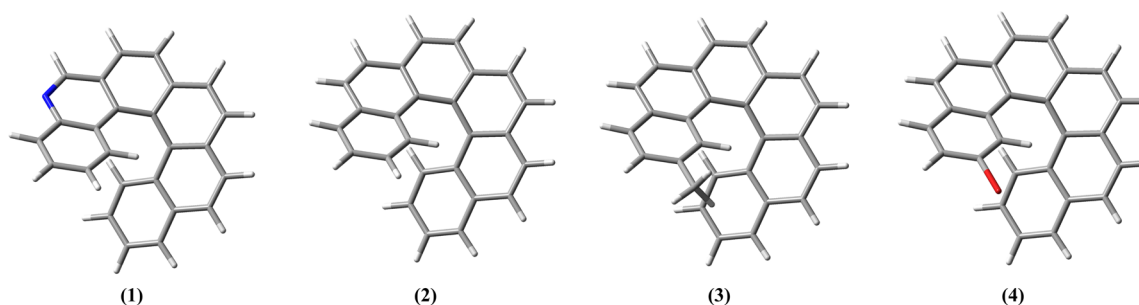
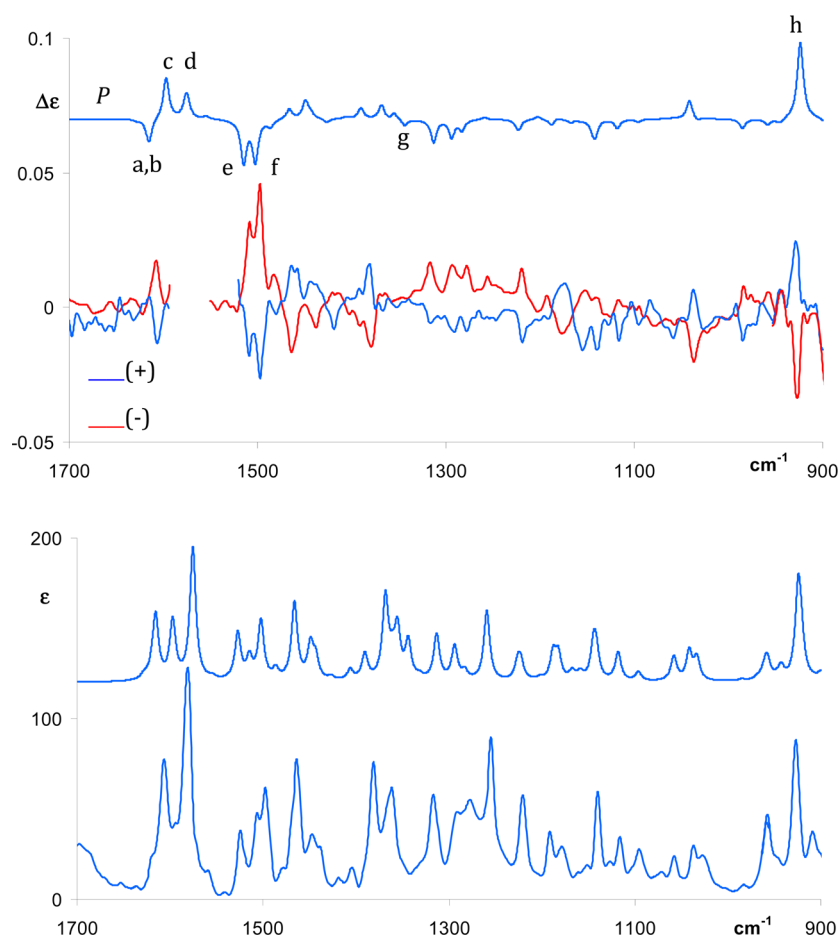[a]Representation taken with Gaussian ancillary code Gaussview.[29].

Figure 1. Comparison of the experimental VCD spectra of both enantiomers of 5-aza-hexahelicene (**1**) with calculated VCD spectra for the *P* enantiomer of **1** in the fingerprint region (top two panels). Comparison of IR absorption experimental and calculated spectra for the *P* enantiomer of **1** in the same spectral region (for experimental conditions and computational details, see text; computed wavenumbers have been scaled). Labels a–h are useful for the discussion in the text and correspond to normal modes of Figure 2

Recently the AC of 2-Br-hexalicene was confirmed also by vibrational circular dichroism (VCD) and density functional theory (DFT) calculations[20] and further determined via Raman optical activity (ROA);[21] further vibrational optical activity (VOA) studies on these compounds can be found in refs 22−26. A few studies had been made in the past on helicene (**2**)[27] employing circularly polarized luminescence (CPL).[28]

Taking advantage of the fact that six-membered helicenes are in all cases enantiomerically stable, in this work we investigate four types of hexahelicenes: 5-aza-hexahelicene (**1**), hexahelicene (**2**), 2-methyl-hexahelicene (**3**), and 2-bromo-hexahelicene (**4**;

see Scheme 1). For them, depending on sample availability, we have run VCD (in the present work we report data for **1**; for **4** this had been done previously[20]); for all four compounds **1**−**4**, ECD and CPL spectra will be provided and interpreted on the basis of current TD-DFT calculations.[19,20,29−32] A unifying view in the interpretation of all spectroscopic data for all the different helicenes has been found in the recent computational works of Inoue et al.,[31,32] who had introduced the useful concepts of helical sense-responsive and substituent-sensitive features for the interpretation of ECD spectra of helicene-based systems (in the course of this writing we will abbreviate the former features as *H*,

and the latter ones as **S**). Since helicity in these systems is strictly connected with conjugation, **H** features owe their intensity to this electronic property, thus one may say that they are also conjugation sensitive. For this reason we extend the notion of **H** and **S** features from the initial domain of electronic spectroscopy[31,32] to the field of vibrational spectroscopy. The distinction, suggested by either similarities or differences among spectra of different compounds, finds a correspondence with the character of the associated normal modes: **H** vibrational features correspond to delocalized normal modes that involve the whole helicene structure; on the contrary, **S** vibrational features exhibit nuclear displacements that are more localized on the given substituent (usually localization is not complete due to vibrational couplings among internal coordinates[33]). Not only do we think that this approach will serve for the discussion of a range of different spectroscopic data, but will also give a rationale, in the future, to design molecules with the best spectroscopic properties for possible optoelectronic applications.

II. RESULTS AND DISCUSSION

a. **H and S Features in VCD Spectra.** In Figure 1 we report the IR and VCD spectra of both enantiomers of 5-aza-hexahelicene **1** in the mid-IR and compare them with the corresponding calculated spectra of the *P* enantiomer. In line with findings reported for all other hexahelicene systems, also for compound **1** we found that the (+) OR sign corresponds to *P* configuration and the (−) sign corresponds to *M* helicity.

Indeed, this choice ensures the best correspondence between the signs and intensities of most of the observed and calculated VCD bands. Let us consider in detail the most intense observed VCD bands and let us analyze the associated normal modes, as presented in Figure 2.

As anticipated in the introduction, we will check delocalization or localization of normal modes in order to define **H** or **S** vibrational features, respectively

(1) Negative VCD feature at 1608 cm^{-1}; it is found close to the strongest IR signal in the mid-IR region, but not coincident with it, rather with the second largest band at higher wavenumbers, and was observed also with the same sign and relative intensity for heptahelicene by Bürgi et al.[22] We had not been able to observe it in 2-Br-hexahelicene due to poor reproducibility of the signal,[20] but in each one of the other two cited cases, similar IR bands were observed. This comparison is in favor of this band having mostly an **H** character. Calculations indicate that the negative band is due to two vibrational features with the same sign so close as to resemble a degenerate pair (modes a and b of Figure 2): they are in-plane HCC bendings coupled to CC stretchings in the inner and in the outer periphery of the molecule. Particularly the b component is a normal mode that is delocalized over the entire structure; in correspondence of the most intense IR peak at about 1580 cm^{-1}, another VCD band is predicted, but we were not able to operate our VCD apparatus there. The normal modes in this region (modes c and d of Figure 2) are fairly delocalized and show an **H** character; using the nomenclature of modes typical of graphene, they correspond to the important Raman G feature[21] (vide infra).

(2) Negative VCD doublet at 1508 and 1499 cm^{-1}; a quite similar doublet was observed in the VCD spectrum of (−)-2-Br-hexahelicene, with opposite sign (*M* config-
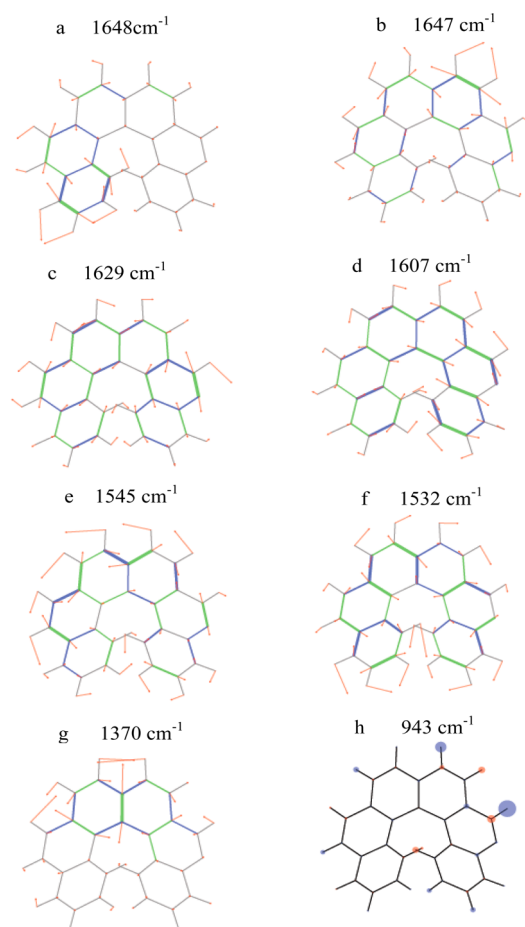

Figure 2. Description of relevant normal modes for 5-aza-hexahelicene in the *P* form (**1**) discussed in the text, which are important to characterize the features of the VCD, IR, and Raman spectra, in Figures 1 and 8. Red arrows represent nuclear displacement vectors; CC bonds are represented as green (blue) lines of different thickness according to their relative stretching (shrinking). For mode h the size of blue/red circles of the molecular sketch is proportional to nuclear displacements in the out-of-plane.

uration) and quite similar intensities.[20] In the case of heptahelicene,[22] we have also a quite similar feature, in shape and sign, even though the two negative components have more unequal VCD intensities. On this basis we definitely assign an **H** character to this doublet; the modes underneath, modes e and f of Figure 2, have still some resemblance to G modes and are mainly HCC bendings coupled to CC stretchings with a relative phase such that half of the molecule is moving opposite to the other. Similar modes were commented for molecule **4**,[20] for which we had also been able to observe on the high frequency side a positive VCD band, which apparently does not show up here. G modes are strictly correlated to D modes (radial CC stretchings, from the nomenclature used for polycyclic aromatics, like graphene), which are calculated here at 1370 cm^{-1} (mode g of Figure 2) and are observed as the most intense peak of the Raman spectrum, with a further relevance in ROA spectra[21] (vide infra). In conclusion, all modes commented above involve the whole conjugated system and, irrespective of substituent and helix length, are helical sensitive, **H**.
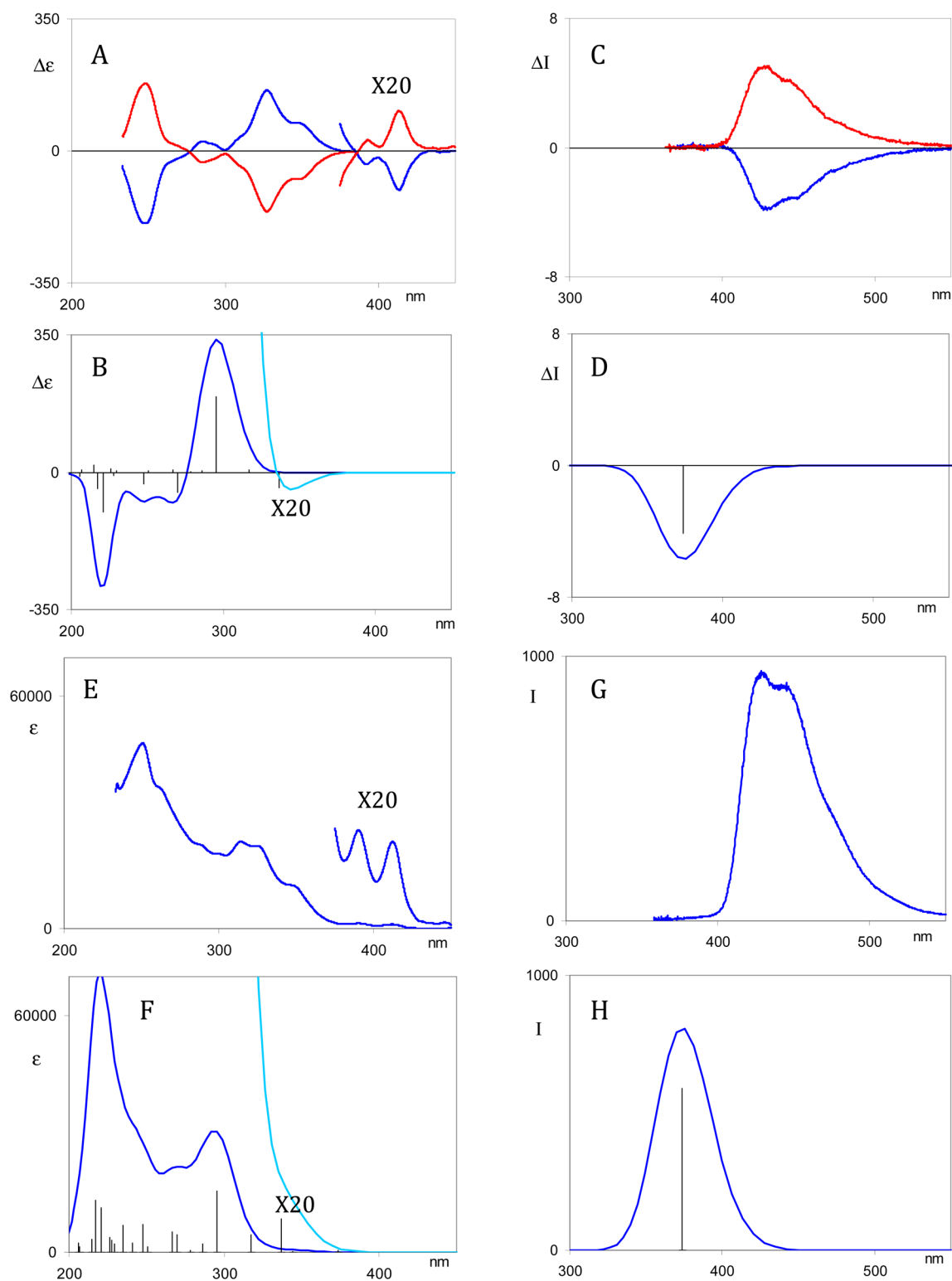
Figure 3. Comparison of experimental ECD spectra of both enantiomers of **1** (5-aza-hexahelicene), panel A, with the DFT calculated ECD spectra of the *P* enantiomer of **1**, panel B (lines proportional to rotational strength for the given transition are superimposed to calculated spectra). Comparison of experimental UV absorption spectra for *P*-**1** (E) with corresponding calculated UV spectra (F; lines proportional to dipole strengths superimposed to calculated spectra). Comparison of experimental CPL spectra of both enantiomers of **1** (5-aza-hexahelicene; C) with the DFT calculated CPL spectra of the *P* enantiomer of **1** (lines proportional to rotational strength for the given transition are superimposed to calculated spectra; D). Comparison of experimental fluorescence spectra for *P*-**1** (G) with corresponding calculated fluorescence spectra (H; lines proportional to dipole strengths superimposed to calculated spectra).

(3) Positive VCD feature at ~930 cm^{-1}; this feature has quite large rotational strength and is in correspondence of a

fairly intense IR band. For molecule **4** we had been unable to observe such a band, but DFT calculations predict a
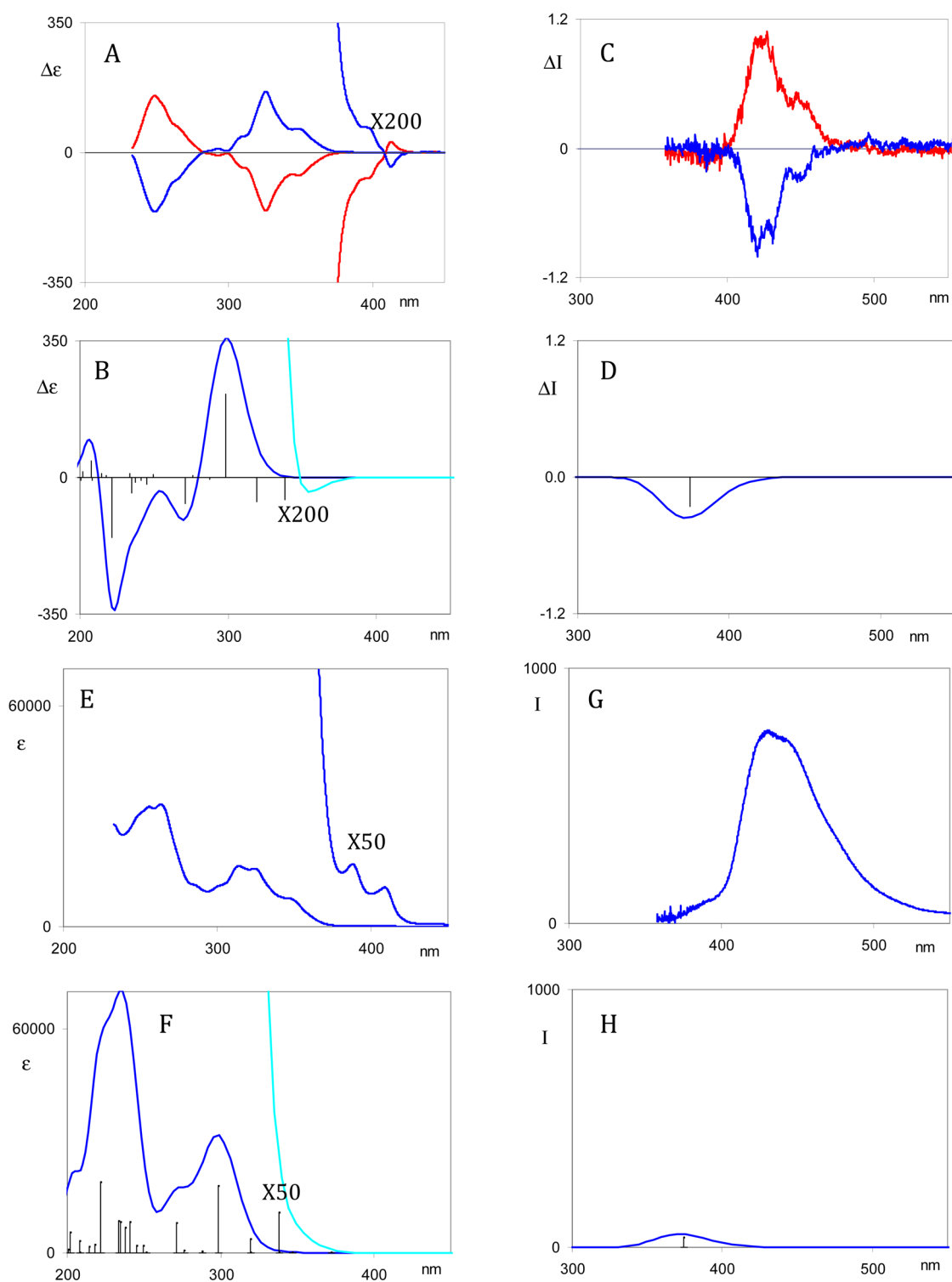
Figure 4. Comparison of experimental ECD spectra of both enantiomers of **2** (hexahelicene; A) with the DFT calculated ECD spectra of the *P* enantiomer of **2** (lines proportional to rotational strength for the given transition are superimposed to calculated spectra; B). Comparison of experimental UV absorption spectra for *P*-**2** (E) with corresponding calculated UV spectra (F; lines proportional to dipole strengths superimposed to calculated spectra). Comparison of experimental CPL spectra of both enantiomers of **2** (hexahelicene; C) with the DFT calculated CPL spectra of the *P* enantiomer of **2** (lines proportional to rotational strength for the given transition are superimposed to calculated spectra; D). Comparison of experimental fluorescence spectra for *P*-**2** (G) with corresponding calculated fluorescence spectra (H; lines proportional to dipole strengths superimposed to calculated spectra).

localized out of plane VCD band at slightly lower frequencies, but with a different magnitude.[21] This leads us to assign mainly an **S** character to this band, and this is clearly seen by looking at the representation of mode h in

Figure 2, where one may appreciate that an out of plane CH bending mode close to the nitrogen is taking place. The special role of CH bonds in proximity of a nitrogen atom in azahelicene molecules has already been pointed
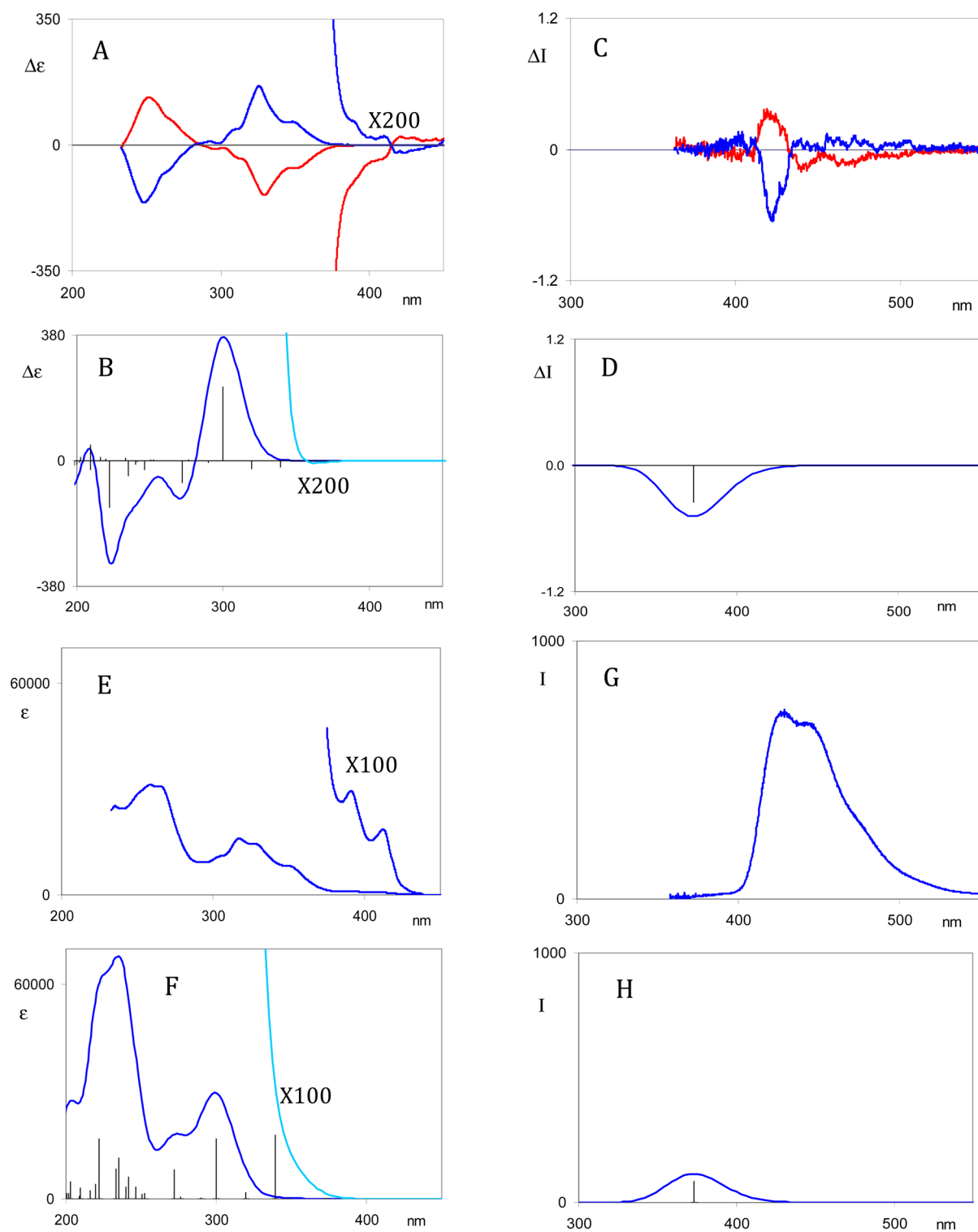
Figure 5. Comparison of experimental ECD spectra of both enantiomers of **3** (2-methyl-hexahelicene) (A) with the DFT calculated ECD spectra of the *P* enantiomer of **3** (lines proportional to rotational strength for the given transition are superimposed to calculated spectra) (B). Comparison of experimental UV absorption spectra for *P*-**3** (E) with corresponding calculated UV spectra (F; lines proportional to dipole strengths superimposed to calculated spectra). Comparison of experimental CPL spectra of both enantiomers of **3** (2-methyl-hexahelicene; C) with the DFT calculated CPL spectra of the *P* enantiomer of **3** (lines proportional to rotational strength for the given transition are superimposed to calculated spectra; D). Comparison of experimental fluorescence spectra for *P*-**3** (G) with corresponding calculated fluorescence spectra (H; lines proportional to dipole strengths superimposed to calculated spectra).

out on the basis of NMR data.[34] Furthermore, in heptahelicene[22] (same helicity as hexahelicene case), the

aspect of this band changes considerably, becoming a bisignate doublet of presumably larger rotational strength.
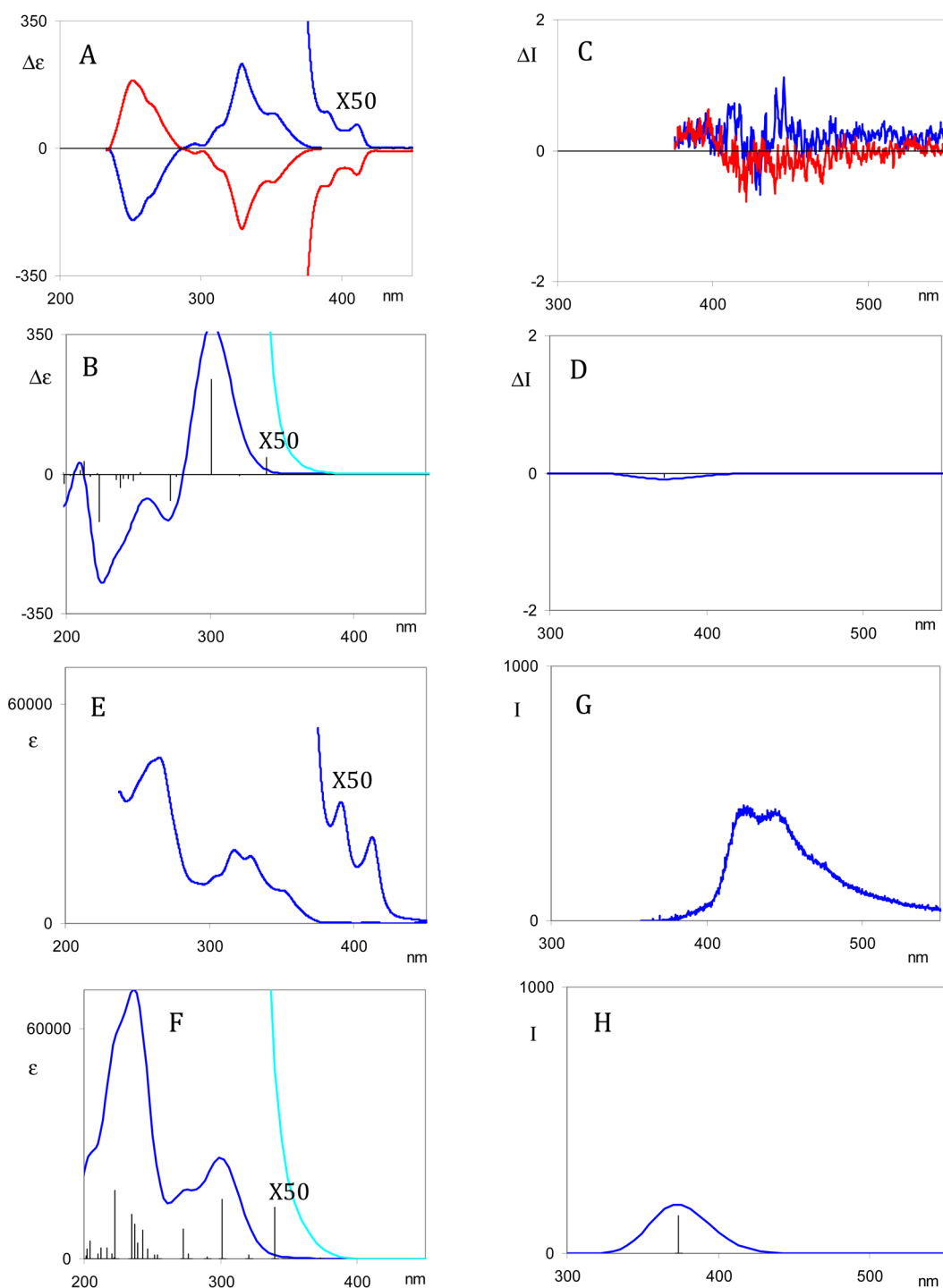
Figure 6. Comparison of experimental ECD spectra of both enantiomers of **4** (2-Br-hexahelicene; A) with the DFT calculated ECD spectra of the *P* enantiomer of **4** (lines proportional to rotational strength for the given transition are superimposed to calculated spectra; B). Comparison of experimental UV absorption spectra for *P*-**4** (E) with corresponding calculated UV spectra (F; lines proportional to dipole strengths superimposed to calculated spectra). Comparison of experimental CPL spectra of both enantiomers of **4** (2-Br-hexahelicene; C) with the DFT calculated CPL spectra of the *P* enantiomer of **4** (lines proportional to rotational strength for the given transition are superimposed to calculated spectra; D). Comparison of experimental fluorescence spectra for *P*-**4** (G) with corresponding calculated fluorescence spectra (H; lines proportional to dipole strengths superimposed to calculated spectra).

b. *H* and *S* Features in ECD and CPL Spectra. In Figures 3−6 we report the comparison of experimental ECD and UV absorption (panels A and E) and of experimental CPL and fluorescence spectra (C and G) of both enantiomers of **1**−**4**, with the corresponding calculated spectra for the *P* enantiomer at CAM-B3LYP/TZVP level (B, F, D, and H). In general, the prediction based on the TDDFT method for the largest ECD features is pretty good, as we had seen earlier on similar systems and as amply proved in the literature.[10,11,31,32,35] Using CAM-B3LYP, the calculated transition wavelengths are lower than observed. We are aware that higher level TD-DFT methods may better represent these systems,[31] however, we had to accept a
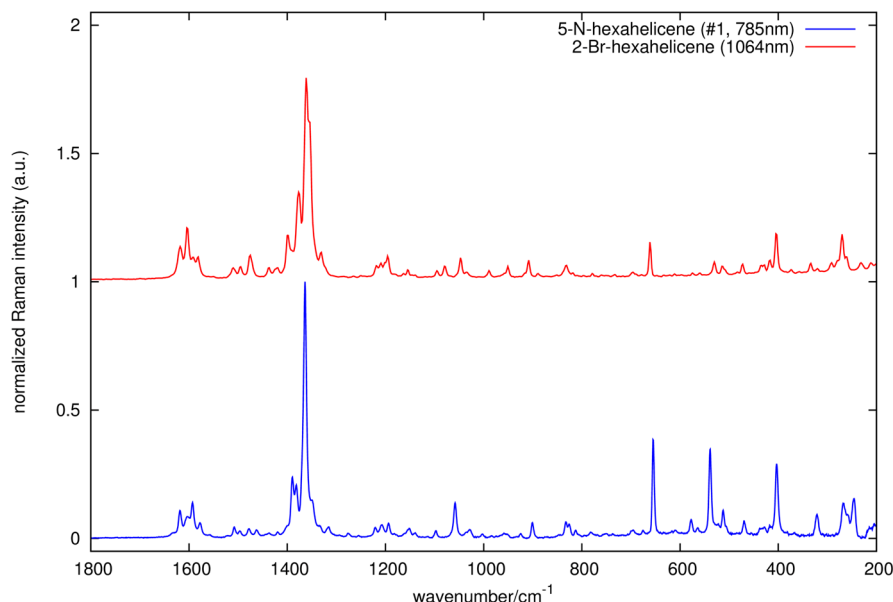
Figure 7. Off-resonance experimental Raman spectra of molecules **1** and **4** (solid state samples in the form of powders).

compromise here since calculation of emission properties (which are at the center of our interest in this work) requires optimization of the excited state, and this is a challenging task from the computational point of view.

One may see that the major experimental features of ECD, absorption and fluorescence spectra of **1**−**4** are quite similar. Minor features in ECD spectra, mainly at long wavelengths, and CPL spectra as a whole are instead significantly different in the four cases. Let us have a closer look at the individual features in order to identify the **H** and **S** features.

(1). 5-Aza-hexahelicene (1). Three ECD bands are worth commenting, namely, the two strong bands at ∼245 nm (− sign for *P* enantiomer) and ∼325 nm (+ sign), and moreover, the 411 nm (− sign) very weak band (Figure 3A), which is a **S**-type band according to Inoue et al.[31,32] (the former two are instead **H**-type features). The major contribution to the lowest energy band is the HOMO → LUMO transition; this is also the one involved in fluorescence and CPL emission. The excited state geometry is similar to that of the ground state, the major differences involving CC bond lengths, while the helical structure is conserved and the electronic transitions are similar in dipole and rotational strengths. This implies that the sign of the CPL band (two likely vibronic features at 427 and 444 nm) is related to the ECD one at 411 nm, as experimentally observed (Figure 3A,C). Calculations both for ECD, CPL, absorption, and fluorescence (Figure 3B,D,F,H) show a good correspondence with experimental data and allow to confirm the above interpretation. In the figure the two low energy absorption and ECD bands are multiplied by a factor of 20; however, the second transition is calculated with nearly zero dipole and rotational strength and is hidden under the nearby intense band (only the bar of the first transition is visible). Moreover, it must be noted that vibronic contributions are not taken into account here and may be important for explaining the features commented above.

(2). Hexahelicene (2). The recorded features in ECD are found at 250 nm (− for *P*) and at 328 nm (+ for *P*) and 412 nm (−) and possibly a (+) feature at 398 nm (Figure 4A). The UV spectrum in the long wavelength region exhibits two peaks in correspondence with the two latter features, namely, at 387 and 408 nm (Figure 4E). The highest wavelength band at about 410

nm is the **S** feature, which is related to the observed CPL broad feature (− for *P*; Figure 4C) with two, possibly vibronic components at 421 and 444 nm (in correspondence with the fluorescence doublet at 426 and 444 nm). Of course the 250 and 328 nm intense ECD features are of type **H**. The calculations again allow to reproduce the UV and ECD spectra in all regions; for CPL the calculated band has the right sign. Investigations regarding vibronic coupling, likely responsible for the shape of the observed emission band, are beyond the scope of this work.

(3). 2-Methyl-hexahelicene (3). The two **H** features are recorded in ECD (Figure 5A) at 251 nm (− for *P*) and at 330 nm (+ for *P*) and a broad very weak feature at 420 nm (−) with possibly two positive (+) ill defined features at ∼410 nm and at ∼390 nm (in the tail of the strong positive 330 nm ECD band); the latter two features appear in correspondence of the better defined UV peaks at 413 and 392 nm (Figure 5E). The CPL spectrum (Figure 5C) is more structured than in the two previous cases: the features have alternating signs, namely, for the *P* isomer we observe a very weak (+) band at 400 nm, a (−) band at 422 nm, which is the most intense one, and a broad (+) band with two features at 440 and 465 nm. Calculations (Figure 5B,D,F,H) are of the same quality as in the two previous cases, namely, while the ECD and UV spectra are quite understood from 200 to 400 nm, the CPL and fluorescence spectra calculations presented here can accout only for one feature, allowing to predict (−) sign for CPL. The multiple features observed in CPL and the double one in fluorescence may still be attributable to vibronic features.

(4). 2-Br-hexahelicene (4). In ECD (Figure 6A) the two **H** features are recorded at 252 nm (− for *P*) and at 329 nm (+ for *P*) while the two weak (+) features observed at 390 and 411 nm (in correspondence with UV absorption, Figure 6E) are once again of **S** type. Fluorescence is quite low as can be inferred by the signal-to-noise ratio, and CPL is confused within the noise (Figure 6G and C, respectively). The fluorescence being so weak has permitted the observation of a Raman and ROA spectrum for this molecule.[21]

Inoue et al.[31,32] pointed out that the **H** and **S** character of a given ECD transition may be theoretically evidenced by plotting the electric and magnetic dipole transition moments and by

Table 1. Transition Wavelength (nm), Dipole Strength (D 10^{-40} esu^2 cm^2), Rotational Strengths (R 10^{-44} esu^2 cm^2) in the Velocity and Length Representations, Magnitude of the Electric and Magnetic Transition Dipoles, $|\langle 0|\mu|e\rangle|$, $|\langle 0|m|e\rangle|$ (atomic units) and Angle Formed by Them (if Lower than 90°, It Corresponds to Positive Rotational Strength)[a]

molecules	λ (nm)	D	R_{vel}	R_{length}	$|\mu|$	$|m|$	angle
1	337	6521	−7.40	−7.01	0.32	0.23	114
	317	3507	1.18	0.89	0.23	0.30	87
	295	237389	738.70	766.32	1.92	4.20	66
	374	**10258**	**−18.00**	**−17.93**	**0.40**	**0.20**	**161**
2	338	1653	−1.08	−0.80	0.16	0.19	96
	319	543	−1.18	−1.18	0.09	0.06	180
	299	271283	816.75	833.62	2.05	4.32	66
	372	**633**	**−1.12**	**−1.00**	**0.10**	**0.07**	**130**
3	339	2740	−0.38	0.13	0.21	0.28	89
	320	272	−0.46	−0.46	0.06	0.04	148
	300	255643	855.02	873.79	1.99	4.42	65
	373	**1428**	**−1.52**	**−1.26**	**0.15**	**0.14**	**105**
4	340	3900	3.17	3.95	0.25	0.46	81
	320	341	−0.28	−0.28	0.07	0.05	109
	301	239751	909.17	928.44	1.93	4.62	64
	373	**2302**	**−0.30**	**0.15**	**0.19**	**0.30**	**89**

[a]The lowest three transitions calculated at the ground state equilibrium structure are reported in normal character; the transition at the optimized structure of the excited state is reported in bold character.

inspecting the angle between them. In Table 1 we report the calculated values for dipole and rotational strengths, electric and magnetic dipole transition moments, and their relative orientation, the latter quantity being responsible of the sign of the rotational strength. These results, obtained from straightforward TDDFT calculations, are meant to offer the zeroth order framework for our understanding. Certainly vibronic coupling may play an important role, especially for very weak electronic transitions like the lowest energy one (L_b for helicene), as pointed out long time ago for instance by Weigang et al.[27] When rotational strengths are too small, their calculated value and sign are not safely determined: this is the case of methyl hexahelicene **3** for ECD and 2-Br-hexahelicene **4** for CPL (this uncertainty is also reflected by the different result obtained in the length and velocity representation; also the experimental observation is not so clear-cut). The weak calculated value of the rotational strength can be traced back to the quasi orthogonality of the electric and magnetic transition dipole vectors (they form an angle of 91° for **3** in ECD and for **4** in CPL). For hexahelicene **2**, the angle for the L_b transition is the same as found in refs 31 and 32 (namely 96°), while for the B_b transition it differs by only 3°.

From Table 1, one may notice how similar are the reported values for the third transition responsible of the H band (B_b for hexahelicene **2**). On the contrary, important differences are observed for the other reported transitions, particularly the ones that are associated with emission. As for the angle, the emission rotational strength should be favored for **1**−**3**; however, magnetic and electric dipole transition moments for compounds **2** and **3** are calculated to be smaller in emission than in absorption. Certainly calculations account for the fact that, among the compounds considered here, 5-azahelicene, **1**, exhibits the largest fluorescence and CPL. In the other cases

both CPL and fluorescence are smaller, though they are experimentally observed for both compounds **2** and **3**.

c. H and S Features in Raman Spectra. As stated above, H bands are connected with conjugation of these molecules. A quite informative technique for π-conjugated systems is Raman spectroscopy. The Raman spectrum of **1** is reported in Figure 7; it has been obtained with NIR excitation at 785 nm; this can be compared with the Raman spectrum of **4** (recorded with NIR excitation at 1064 nm). The spectra of the two enantiomers of **1**, even if excited with NIR laser, show some fluorescence background however weak enough to allow for reliable baseline correction (see Figure SI1). Overall, the two Raman spectra exhibit a similar pattern: two characteristic and structured Raman signals are found in the neighborhood of 1350 and 1600 cm^{-1}, which had been respectively assigned to D and G modes in compound **4**, for which they had been characterized also at ROA.[21]

Those features, which are similar in the Raman spectra of **1** and **4** are associated to delocalized conjugation sensitive modes, coincident, in these systems, with H features. On the opposite, the bands that appear in just one of the two spectra or whose intensities are quite different for the two compounds, partake of S character. DFT calculations further help to define this aspect (for completeness also the calculated Raman spectrum for hexahelicene **2** is reported, see Figure 8). Moreover, the D peak in **1**, **2**, and **4** is calculated almost at the same wavenumber (ca. 1370 cm^{-1}) with similar Raman intensity and similar nuclear displacement patterns (localized in the central ring of the hexahelicene backbone, see Figure 8): this fact leads us to conclude that it is of the H type.

DFT also allows one to check that the higher wavenumber Raman mode in the G region (close to 1660 cm^{-1}) is sensitive to
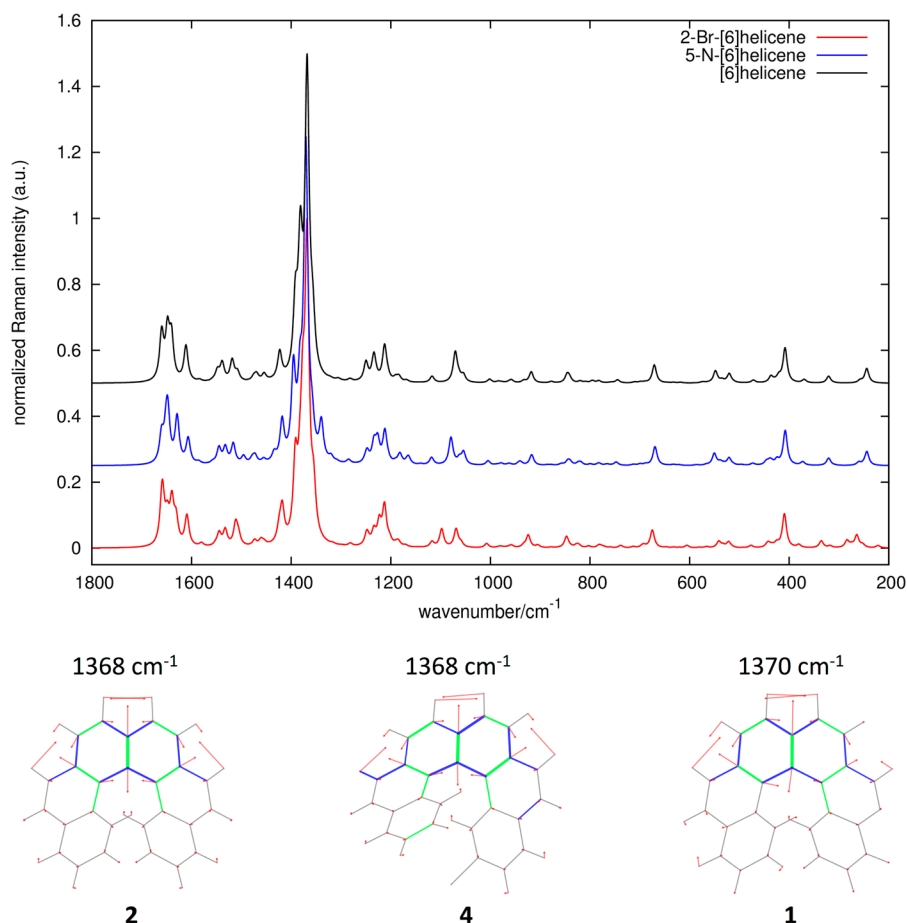
Figure 8. Top: simulated off-resonance Raman spectra of **2**, **1**, and **4**. Bottom: nuclear displacements corresponding to the D peak in **2**, **1**, **4**. These data have been obtained from DFT calculations at B3LYP/TZVP level (unscaled wavenumbers).

substitution in a peculiar way. In unsubstituted hexahelicene **2** it is a degenerate doublet at 1660 cm^{-1}. Upon methyl substitution, compound **3**, the degeneracy is very weakly lifted (1660 and 1658 cm^{-1}) with nuclear displacements localized on the two halves of the molecule (see Figure SI2). The case of the nitrogen substitution along the π-conjugated helix, **1**, is more interesting: one component of the doublet (at 1660 cm^{-1}) is localized on the half of the molecule not bearing the nitrogen atom (see also Figure 2g), the other component involves the part with the nitrogen atom, which affects the vibrational dynamics and shifts the wavenumber to 1651 cm^{-1} (see Figure SI3). This analysis leads us to conclude that the G mode is potentially more influenced by substitution (see also part a of this section). However, a comparison of the three simulated Raman spectra in Figure 8 does not reveal any straightforward marker of substitution in the G region but rather subtle changes of the spectral shape. Similarly, even if the D peak is remarkably stable upon substitution, the shoulders and side peaks in the D region are affected to some extent by substitution of the hexahelicene backbone. Notably, in **1** a peak at 1339 cm^{-1} stands out in the lower wavenumber wing of the D peak (see Figure 8). The associated normal mode has the typical D-mode pattern and is localized on the end ring close to nitrogen. Hence, this mode is affected by the perturbation caused by the heteroatom in the hexahelicene backbone. Comparison with experimental data allows to assign this feature to the peak measured at 1333 cm^{-1}, which is however relatively weaker than predicted by DFT (see Figure SI4).

Finally, below 800 cm^{-1}, a series of Raman lines is found in compounds **1** and **4** at similar frequencies (see Figures 7 and SI5 for further details). Among those, the collective helical breathing, discussed in ref 21, is measured at 402 and 410 cm^{-1} for **1** and **4**, respectively. Hence, this mode also is weakly sensitive to substitution. Major differences between **1** and **4** are observed in particular considering the peak computed at 550 cm^{-1} for **1** (expt 538 cm^{-1}), which is not observed with the same prominence in **4** (where it red shifts at 530 cm^{-1} − see Figure 7) .

III. CONCLUSIONS

In this work we have measured the ECD, UV, fluorescence, and CPL spectra of four simple hexahelicene molecules. For one of the compounds, namely, 5-aza-hexahelicene **1**, we were able to measure VCD and Raman spectra, while for 2-Br-hexahelicene **4** these two forms of spectroscopies had been applied previously.[20,21] In all molecules we have been able to find VCD, Raman, and ECD signatures which are invariant with addition of the different substituents examined, that is, are associated with the conjugated backbone: following Inoue et al.[31,32] we have named them helicity features **H**. Other features instead are dependent on the substituent (**S** features). The CPL spectra are determined by a single electronic transition, whose sign and strength is dependent on substituent, thus making CPL spectra entirely of **S** character.

The DFT calculations have allowed to confirm these findings, which were obtained on a solid correlative basis: in the case of ECD and CPL, TDDFT methodology differentiates **H** from **S**

Scheme 2. Schematics of the Synthesis and Photosynthesis Steps to Obtain 5-Aza-hexahelicene (1)
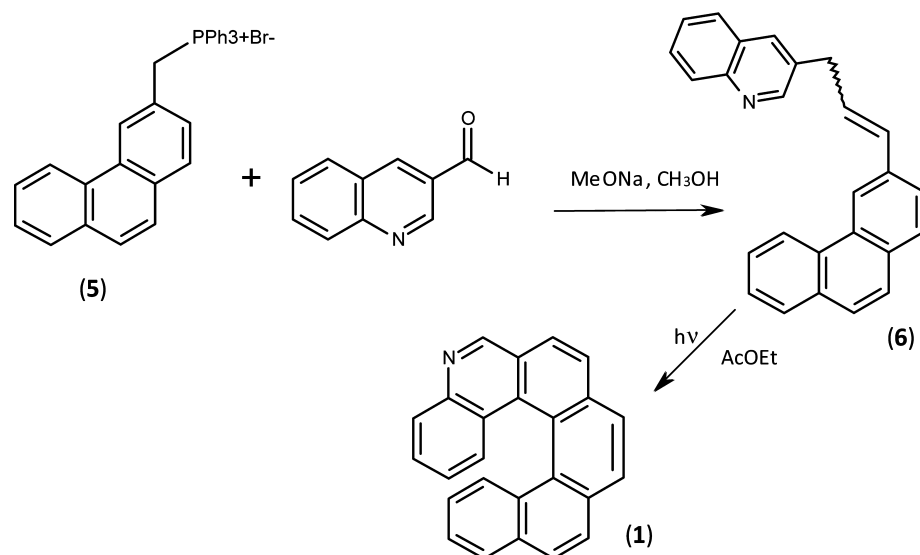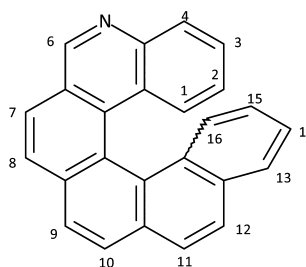

Table 2. ^{1}H NMR Signals for Compound (1)^a

δ (ppm)	Mult.	ass.	J1 (Hz)	J2 (Hz)	J3 (Hz)
9.50	s	H6	-	-	-
8.14	dd	H4	8.25	1.50	-
8.12	A of AB	H7/H8	8.20	-	-
8.11	B of AB	H8/H7	8.20	-	-
8.08	A of AB	H10	8.25	-	-
8.03	B of AB	H8	8.25	-	-
7.99	A of AB	H12	8.58	-	-
7.95	B of AB	H11	8.58	-	-
7.88	dd	H13	8.10	1.50	-
7.63	dd (br)	H16	8.50	0.8	-
7.48	dd	H1	8.50	1.50	
7.40	ddd	H3	6.90	1.50	8.25
7.29	ddd	H14	6.90	1.25	8.10
6.77	ddd	H15	6.90	1.50	8.50
6.74	ddd	H2	6.90	1.50	8.50

^{a}In the figure, numbering of the skeletal positions is reported.

through calculation of the angle between electric and magnetic dipole transition moments (either far or close to 90°); in the case of VCD, IR, and Raman, DFT allows to differentiate **H** from **S** by checking normal modes delocalization or localization, respectively.

IV. EXPERIMENTAL AND COMPUTATIONAL METHODS

General Procedures. ^{1}H and ^{13}C NMR spectra were recorded in CDCl$_3$ on Varian INOVA 400 MHz and Bruker Avance 500 MHz spectrometers using TMS as internal standard. Column chromatography was carried out using Macherey-Nagel silica gel 60 (70−230 mesh). Analytical thin-layer chromatography (TLC) was performed on Macherey-Nagel aluminum sheets precoated with silica gel (0.25 mm). Tetrahydrofuran (THF) was freshly distilled prior to its use on sodium benzophenone ketyl and stored under nitrogen atmosphere. MeLi (1.6 M in diethyl ether) and t-BuLi (1.5 M in pentane) were used as purchased (Aldrich). The other commercially available chemicals (Sigma-Aldrich) were used as received. GC-MS analyses were performed either on a Hewlett-Packard 6890 chromatograph equipped with an HP-5973 mass detector or on an Agilent 6850 chromatograph equipped with an Agilent 5975N

mass detector. HPLC separations were carried on a JASCO PU-1580 pump with a Varian 2550 UV detector.

(a). Synthesis and Enantiomer Separation of 5-Aza-hexahelicene (1). The synthesis of this product was approached following the same strategy used for analogous monoaza-pentahelicenes,[36] as depicted in Scheme 2.

The phosphonium salt **5** was prepared as described in ref 36 and was used for a Wittig condensation with an equimolar amount of commercial quinoline-3-carboxaldehyde, using 3 equiv of MeONa in refluxing methanol during 6 h and obtaining product **6**. After cooling down, 30 mL of water were added to the reaction mixture. The organic phase was then extracted three times with a total of 100 mL of CH$_2$Cl$_2$. Compound **6**, which forms as a mixture of the *cis*- and *trans*-isomers, was purified by silica gel chromatography by eluting with a 1:1 hexane−ethyl acetate mixture, affording a 50% isolated yield of the isomeric mixture. Compound **6** was then dissolved in ethyl acetate (concentration 0.5 g/L) and irradiated with visible light during 24 h in Pyrex vessels, yielding azahelicene **1**, which was then purified by silica gel chromatography. The eluting mixture was 1:1 hexane−ethyl acetate, the isolated yield was 53%, the recovery of unreacted product **6** was 20%. The compound appeared as a light yellow crystalline solid with mp 250−252 °C.

Compound **1** was characterized by mass spectroscopy (*m/z* 329, 314, 302, 163) and by ¹H NMR in CDCl₃ (Table 2).

The enantiomers of 5-aza-hexahelicene **1** were resolved by semipreparative HPLC using a Chiralpak-IA column (250 × 10 mm I.D.), *n*-hexane/2-propanol 97/3 as eluent (flow rate 5 mL/min and T 25 °C) and UV detection at 280 nm. The sample was dissolved in chloroform/mobile phase 60/40 (*c* = 12 mg/mL) and 200 *μ*L (2.4 mg) were injected for each run (process yield 95%). The enantiomeric excess of the collected and pooled fractions was checked by analytical HPLC using a Chiralpak-IA column (250 × 4.6 mm I.D.) under the same conditions used for semipreparative mode, except for the flow rate (1 mL/min). For each enantiomer we obtained about 12 mg with e.e. = 99.0% (see Figure SI6 for further details). Polarimetric measurements on the second eluted enantiomer gave $[\alpha]_D^{25}$ = −3241° (*c* 0.002, CHCl₃).

(b). Synthesis of (±)-2-Bromohexahelicene (4). Racemic 2-bromohexahelicene (**4**) was prepared as previously reported.[7,8]

MS (EI): *m/z* 408 (M⁺, 77), 406 (77), 327 (49), 326 (91), 325 (56), 324 (69), 301 (30), 300 (100), 163 (63), 162 (89), 161 (36), 150 (23), 149 (23). ¹H NMR (400 MHz, CDCl₃): δ 7.84−8.03 (m, 9H), 7.73 (s, 1H), 7.65−7.67 (d, *J* = 8.40, Hz, 1H), 7.54−7.56 (d, *J* = 8.80 Hz, 1H), 7.25−7.32 (m, 2H), 6.71−6.75 (m, 1H). ¹³C NMR (100 MHz, CDCl₃): δ 133.3, 132.4, 131.8, 131.7, 131.2, 130.7, 130.4, 129.8, 129.1, 128.7, 128.4, 128.1, 127.8, 127.7, 127.6, 127.5, 127.3, 127.2, 127.1, 127.0, 126.9, 126.4, 126.2, 124.9, 124.1, 119.3.

(c). Synthesis of (±)-Hexahelicene (2). To a solution of (±)-**4** (100 mg; 0.250 mmol) in anhydrous THF (5 mL) *t*-BuLi (1.5 M, 833 *μ*L, 1.25 mmol) was added at 0 °C under nitrogen. The mixture was stirred for 2 h and then quenched with 10% saturated aqueous NH₄Cl. The aqueous phase was extracted with ethyl acetate and the collected organic phases were dried over anhydrous Na₂SO₄. After evaporation of the solvent product **2** was obtained as a yellow solid (71.0 mg, 86%).

MS (EI): *m/z* 328 (M⁺, 100), 327 (26), 326 (25), 324 (27), 301 (43), 300 (77), 162 (29), 156 (23). ¹H NMR (400 MHz, CDCl₃): δ 7.96−8.01 (m, 4H), 7.90−7.95 (m, 4H), 7.83−7.88 (d, *J* = 8.00 Hz, 2H), 7.57−7.59 (d, *J* = 8.60 Hz, 2H), 7.19−7.23 (dd, *J* = 7.70, 7.20 Hz, 2H), 6.65−6.69 (m, 2H).

(d). Synthesis of (±)-2-Methylhexahelicene (3). To a solution of (±)-**4** (50.0 mg; 0.125 mmol) in anhydrous THF (2.5 mL), MeLi (1.6 M, 0.235 *μ*L, 0.375 mmol) was added at 0 °C under nitrogen. The mixture was stirred for 30 min and then quenched with 10% aqueous HCl. The aqueous phase was extracted with ethyl acetate and the collected organic phases were dried over anhydrous Na₂SO₄. After evaporation of the solvent, product **3** was obtained as a yellow solid (41.0 mg, 96%).

MS (EI): *m/z* 342 (M⁺, 100), 327 (38), 326 (35), 300 (46), 162 (25). ¹H NMR (400 MHz, CDCl₃): δ 7.92−8.02 (m, 6H), 7.82−7.89 (m, 2H), 7.80−7.82 (d, *J* = 8.40 Hz, 1H), 7.69−7.71 (d, *J* = 8.08 Hz, 1H), 7.58−7.60 (d, *J* = 8.40, Hz, 1H), 7.36 (s, 1H), 7.21−7.23 (d, *J* = 7.60 Hz, 1H), 7.03−7.05 (d, *J* = 8.08 Hz, 1H), 6.65−6.69 (m, 1H), 1.75 (S, 3H).

(e). Enantiomeric Separation of Hexahelicene (2) and 2-Methylhexahelicene (3). The racemic mixtures of **2** and **3** were resolved by HPLC on a Daicel Chiralcel OD-H chiral stationary phase (c.s.p.), employing hexane/2-propanol (99:1) mixture as mobile phase (flow = 1 mL/min) and peak detection at λ = 254 nm. HPLC of compound (±)-**2** on the c.s.p. provided two peaks, the first eluted one at t_R = 7.1 min, corresponding to the (−)-**2** enantiomer and the second eluted at t_R = 10.2 min, assigned to (+)-**2** (see Figure SI7). Both eluted enantiomers were collected

providing 1.0 mg of (−)-**2** in 98% ee and 1.2 mg of (+)-**2** in 98% ee. Chiral HPLC separation of (±)-**3** provided two peaks, the first eluted one at t_R = 5.1 min assigned to (−)-**3** and the second eluted at t_R = 8.9 min assigned to (+)-**3** enantiomer (see Figure SI7). Both eluted enantiomers were collected providing 0.9 mg of (−)-**3** in 98% ee and 1.2 mg of (+)-**3** in 98% ee.

(f). IR and VCD Measurements. IR and VCD measurements of **1** were carried out on a Jasco FVS6000 apparatus equipped with a ZnSe Photo-Elastic Modulator (PEM) and a MCT detector. The 0.04 M/CDCl₃ solutions for both enantiomers were prepared and 500 *μ*m BaF₂ fixed-path cells were employed for the measurements. Several series of 2000 scans were acquired and averaged; PEM was centered at two different wavenumber values, 1200 and 1600 cm⁻¹, depending on the investigated spectroscopic regions.

(g). FT-Raman Measurements. Micro-Raman measurements were carried out on crystalline powders of the two enantiomers of **1** in off-resonance conditions. The dispersive Raman spectrometer used in our experiments was a Jobin Yvon LABRAM HR800 equipped with a solid state laser (Laser XTRA, Toptica Photonics, 785 nm) and a Peltier cooled CCD detector. The instrument was coupled with a Olympus BX41 microscope using a 50× objective. In our experimental setup the laser power at the sample was less than 10 mW and the focusing area was close to 1 *μ*m².

(h). CPL and ECD Measurements. Identical solutions were used first for ECD and then for CPL measurements, namely, 0.12 mM/CHCl₃ for **1**, 0.15 mM/CHCl₃ for **2**, 0.18 mM/CHCl₃ for **3**, and 0.14 mM/CHCl₃ for **4**. A Jasco 815SE apparatus was employed for ECD measurements. Solutions were contained in 2 mm (or 1 cm, when needed) quartz cuvettes and 10 scans (time constant = 2 s, monochromator velocity 100 nm/min) were taken for each sample of the two enantiomers. For CPL we employed the homemade instrument that we had designed, built, and described in previous papers;[30,37] the excitation radiation was brought to the cell from a Jasco FP8200 fluorimeter through an optical fiber containing water. In all cases the excitation wavelength was set at 350 nm; a 90° scattering geometry was chosen and 5−10 scans were taken for each enantiomer, depending on signal intensity. A microfluorescence quartz cuvette 2 × 10 mm has been used. Spectral response has been corrected using quinine sulfate as a standard.

(i). DFT Calculations. Density functional calculations have been carried out with Gaussian09 quantum chemistry code[29] adopting B3LYP functional and TZVP basis set. The choice was made on the basis of our previous experience on VCD and ROA of 2-Br-hexahelicene **4**.[20,21] IR, VCD, and Raman spectra of **1** have been simulated as superposition of Lorentzian functions centered at the computed vibrational wavenumbers and with an area proportional to the intensities determined by DFT calculations. Lorentzian line width was assumed equal to 8 cm⁻¹ (10 cm⁻¹ for Raman spectra). To further facilitate comparison of observed and calculated spectra, we applied a scaling factor equal to 0.98 to the calculated frequencies. In-house custom codes have been developed and used for the analysis and graphical representation of the vibrational normal modes.

In order to calculate ECD and CPL, molecular structures have been optimized in their ground and first excited states at CAM-B3LYP/TZVP level and transition energies, dipole and rotational strengths have been calculated by TD-DFT. A constant bandwidth of 0.2 eV was applied to each transition. Emission

bands are calculated as reported in ref 30 and analogously to refs 38 and 39.

ASSOCIATED CONTENT

● Supporting Information

Figure SI1, baseline correction of experimental Raman spectra of **1**; Figure SI2, nuclear displacements of Raman modes in the G-peak region of compound **4**; DFT calcs; Figure SI3, nuclear displacements of Raman modes in the G-peak region of compound **1**, DFT calcs; Figure SI4, details of D peak region of Raman spectrum of **1**; Figure SI5, details of low-frequency region of Raman spectrum of **1**; Figure SI6, HPLC diagram of compound **1**; Figure SI7, HPLC diagram of compounds **2** and **3**. This material is available free of charge via Internet.

AUTHOR INFORMATION

Corresponding Author
*E-mail: abbate@med.unibs.it.

Notes
The authors declare no competing financial interest.

ACKNOWLEDGMENTS

REFERENCES

(1) Newman, M. S.; Lutz, W. B.; Lednicer, D. A New Reagent for Resolution by Complex Formation; The Resolution of Phenanthro-[3,4-c]Phenanthrene. *J. Am. Chem. Soc.* **1955**, *77*, 3420−3421.

(2) Newman, M. S.; Lednicer, D. The Synthesis and Resolution of Hexahelicene. *J. Am. Chem. Soc.* **1956**, *78*, 4765−4770.

(3) Newman, M. S.; Darlak, R. S.; Tsai, L. Optical Properties of Hexahelicene. *J. Am. Chem. Soc.* **1967**, *89*, 6191−6193.

(4) Moscowitz, A. On Optical Activity- Hexahelicene. *Ph.D. Thesis*, Harvard University, Cambridge, MS, 1957.

(5) Moscowitz, A. Theoretical Aspects of Optical Activity. Part One: Small Molecules. In *Adv. Chem. Phys.*; Prigogine, I., Ed.; J. Wiley and Sons: New York, 1962; Vol. *IV*, pp 67−112.

(6) Rosenfeld, L. Quantenmechanische Theorie der Natürlichen Optischen Aktivitä̈ von Flüssigkeiten und Gasen. *Z. Phys.* **1928**, *52*, 161−174.

(7) Lightner, D. A.; Hefelfinger, D. T.; Frank, G. W.; Powers, T. W.; Trueblood, K. N. Absolute Configuration of Hexahelicene. *Nature* **1971**, *232*, 124−125.

(8) Lightner, D. A.; Hefelfinger, D. T.; Powers, T. W.; Frank, G. W.; Trueblood, K. N. Hexahelicene. The Absolute Configuration. *J. Am. Chem. Soc.* **1972**, *94*, 3492−3497.

(9) Frank, G. W.; Hefelfinger, D. T.; Lightner, D. A. The Crystal and Molecular Structure of 2-Methylhexahelicene. *Acta Crystallogr.* **1973**, *B29*, 223−230.

(10) Hansen, A. E.; Bak, K. L. Ab Initio Calculations of Electronic Circular Dichroism. *Enantiomer* **1999**, *4*, 455−476.

(11) Furche, E.; Ahlrichs, R.; Wachsmann, C.; Weber, E.; Sobank, A.; Vögtle, F.; Grimme, S. Circular Dichroism of Helicenes Investigated by Time-Dependent Density Functional Theory. *J. Am. Chem. Soc.* **2000**, *122*, 1717−1724.

(12) Laarhoven, W. H.; Prinsen, W. J. C. Carbohelicenes and Heterohelicenes. *Top. Curr. Chem.* **1984**, *125*, 63−130.

(13) Meurer, K. P.; Vogtle, F. Helical Molecules in Organic-Chemistry. *Top. Curr. Chem.* **1985**, *127*, 1−76.

(14) Katz, T. J. Syntheses of Functionalized and Aggregating Helical Conjugated Molecules. *Angew. Chem., Int. Ed.* **2000**, *39*, 1921−1923.

(15) Míšek, J.; Teplý, F.; Stará, I. G.; Tichý, M.; Šaman, D.; Císařová, I.; Vojtíšek, P.; Starý, I. A Straightforward Route to Helically Chiral N-Heteroaromatic Compounds: Practical Synthesis of Racemic 1,14-Diaza[5]helicene and Optically Pure 1- and 2-Aza[6]helicenes. *Angew. Chem., Int. Ed.* **2008**, *47*, 3188−3191.

(16) Urbano, A. Recent Developments in the Synthesis of Helicene-Like Molecules. *Angew. Chem., Int. Ed.* **2003**, *42*, 3986−3989.

(17) Caronna, T.; Sinisi, R.; Catellani, M.; Luzzati, S.; Abbate, S.; Longhi, G. Photochemical Synthesis and Optical Properties of High Membered Thiohelicenes. *Synth. Met.* **2001**, *119*, 79−80.

(18) Lebon, F.; Longhi, G.; Gangemi, F.; Abbate, S.; Priess, J.; Juza, M.; Bazzini, C.; Caronna, T.; Mele, A. Chiroptical Properties of Some Monoazapentahelicenes. *J. Phys. Chem. A* **2004**, *108*, 11752−11761.

(19) Abbate, S.; Bazzini, C.; Caronna, T.; Fontana, F.; Gangemi, F.; Lebon, F.; Longhi, G.; Mele, A.; Natali Sora, I. Experimental and Calculated Circular Dichroism Spectra of Monoaza[5]helicenes. *Inorg. Chim. Acta* **2007**, *360*, 908−912.

(20) Abbate, S.; Lebon, F.; Longhi, G.; Fontana, F.; Caronna, T.; Lightner, D. A. Experimental and Calculated Vibrational and Electronic Circular Dichroism Spectra of 2-Br-Hexahelicene. *Phys. Chem. Chem. Phys.* **2009**, *11*, 9039−9043.

(21) Johannessen, C.; Blanch, E. W.; Villani, C.; Abbate, S.; Longhi, G.; Agarwal, N. R.; Tommasini, M.; Ligthner, D. A. Raman and ROA Spectra of (−)- and (+)-2-Br-Hexahelicene: Experimental and DFT Studies of a π-Conjugated Chiral System. *J. Phys. Chem. B* **2013**, *117*, 2221−2230.

(22) Bürgi, T.; Urakawa, A.; Behzadi, B.; Ernst, K. H.; Baiker, A. The Absolute Configuration of Heptahelicene: A VCD Spectroscopy Study. *New J. Chem.* **2004**, *28*, 332−334.

(23) Nafie, L. A. *Vibrational Optical Activity: Principles and Applications*; Wiley: New York, 2011.

(24) Nafie, L. A.; Freedman, T. B. Vibrational Optical Activity Theory. In *Circular Dichroism Principles and Applications*; Berova, N., Nakanishi, K., Woody, R.W., Eds.; Wiley-VCH: New York, 2000; pp 97−132.

(25) Barron, L. D. *Molecular Light Scattering and Optical Activity*, Cambridge Univ. Press: Cambridge, U.K., 1982.

(26) Barron, L. D.; Hecht, L. Vibrational Raman Optical Activity: From Fundamentals to Biochemical Applications. In *Circular Dichroism Principles and Applications*; Berova, N., Nakanishi, K., Woody, R.W., Eds.; Wiley-VCH: New York, 2000; pp 667−701.

(27) Weigang, O. E., Jr.; Turner, J. A.; Trouard, P. A. Emission Polarization and Circular Dichroism of Hexahelicene. *J. Chem. Phys.* **1966**, *45*, 1126−1134.

(28) Dekkers, H. P. J. M. Circularly Polarized Luminescence: a Probe for Chirality in the Excited State. In *Circular Dichroism: Principles and Applications*, 2nd ed.; Berova, N., Nakanishi, K., Woody, R. A., Eds.; John Wiley & Sons: New York, 2000; pp 185−215.

(29) Frisch, M. J.; Trucks, G. W.; Schlegel, H. B.; Scuseria, G. E.; Robb, M. A.; Cheeseman, J. R.; Scalmani, G.; Barone, V.; Mennucci, B.; Petersson, G. A. et al. *Gaussian 09*, Revision A.02; Gaussian, Inc.: Wallingford, CT, 2009.

(30) Longhi, G.; Castiglioni, E.; Abbate, S.; Lebon, F.; Lightner, D. A. Experimental and Calculated CPL Spectra and Related Spectroscopic Data of Camphor and Other Simple Chiral Bicyclic Ketones. *Chirality* **2013**, *25*, 589−599.

(31) Nakai, Y.; Mori, T.; Inoue, Y. Circular Dichroism of (Di)methyl- and Diaza[6]helicenes. A Combined Theoretical and Experimental Study. *J. Phys. Chem. A* **2013**, *117*, 83−89.

(32) Nakai, Y.; Mori, T.; Inoue, Y. Theoretical and Experimental Studies on Circular Dichroism of Carbo[n]helicenes. *J. Phys. Chem. A* **2012**, *116*, 7372−7385.

(33) Wilson, Jr., E. B.; Decius, J. C.; Cross, P. C. *Molecular Vibrations*, Van Nostrand: New York, NY, 1955.

(34) Caronna, T.; Castiglione, F.; Famulari, A.; Fontana, F.; Malpezzi, L.; Mele, A.; Mendola, D.; Natali Sora, I. Quantum Mechanics

Calculations. Basicity and Crystal Structure: The Role of Transition Metal Complexes of Azahelicenes. *Molecules* **2012**, *17*, 463−479.

(35) Lebon, F.; Longhi, G.; Gangemi, F.; Abbate, S.; Priess, J.; Juza, M.; Bazzini, C.; Caronna, T.; Mele, A. Chiroptical Properties of Some Mono-aza-pentahelicenes. *J. Phys. Chem. A* **2004**, *108*, 11752−11761.

(36) Abbate, S.; Bazzini, C.; Caronna, T.; Fontana, F.; Gambarotti, C.; Gangemi, F.; Longhi, G.; Mele, A.; Natali Sora, I.; Panzeri, W. Monoaza[5]helicenes. Part 2: Synthesis, Characterisation and Theoretical Calculations. *Tetrahedron* **2006**, *62*, 139−148.

(37) Castiglioni, E.; Abbate, S.; Longhi, G. Revisiting with Updated Hardware an Old Spectroscopic Technique: Circularly Polarized Luminescence. *Appl. Spectrosc.* **2010**, *64*, 1416−1419.

(38) Pecul, M.; Ruud, K. The Optical Activity of Beta, Gamma-Enones in Ground and Excited States Using Circular Dichroism and Circularly Polarized Luminescence. *Phys. Chem. Chem. Phys.* **2011**, *13*, 643−650.

(39) Pritchard, B.; Autschbach, J. Calculation of Vibrationally Resolved Circularly Polarized Luminescence of d-Camphorquinone and (*S,S*)-*trans*-*β*-Hydrindanone. *ChemPhysChem* **2010**, *11*, 2409−2415.